

Rapid assembly of high-Mg andesites and dacites by magma mixing at a continental arc stratovolcano

Chris E. Conway^{1,2}, Katy J. Chamberlain³, Yumiko Harigane⁴, Daniel J. Morgan⁵ and Colin J.N. Wilson⁶

¹Research Institute of Earthquake and Volcano Geology, Geological Survey of Japan, AIST, 1-1-1 Higashi, Tsukuba, Ibaraki 305-8567, Japan

²Department of Geology and Paleontology, National Museum of Nature and Science, 4-1-1 Amakubo, Tsukuba, Ibaraki 305-0005, Japan

³School of Environmental Science, University of Derby, Kedleston Road, Derby DE22 1GB, UK

⁴Institute of Geology and Geoinformation, Geological Survey of Japan, AIST, 1-1-1 Higashi, Tsukuba, Ibaraki 305-8567, Japan

⁵School of Earth and Environment, University of Leeds, Leeds LS2 9JT, UK

⁶School of Geography, Environment and Earth Sciences, Victoria University of Wellington, PO Box 600, Wellington 6140, New Zealand

ABSTRACT

Studies of pre-eruptive processes at active volcanoes require precise petrochronological constraints if they are to contribute to hazard assessment during future eruption events. We present petrological and geochemical data and orthopyroxene diffusion time scales for samples from Late Pleistocene high-Mg andesite-dacite lavas (Mg# 53–69) at Ruapehu volcano, New Zealand, as a case study of rapid magma genesis and eruption at a continental arc stratovolcano. Assembly of Ruapehu high-Mg magmas involved the mixing of primitive magmas plus entrained mantle-equilibrated olivines with mid-crustal felsic mush bodies, yielding hybridized magmas with ubiquitous pyroxene reverse-zoning patterns. Orthopyroxene Fe-Mg interdiffusion time scales linked to quantitative crystal orientation data show that most lavas erupted <10 days after resumption of crystal growth following magma mixing events. The eruption of lavas within days of mixing events implies that pre-eruptive warnings may be correspondingly short.

INTRODUCTION

Arc stratovolcanoes are active foci for research on the generation of intermediate-composition magmas and their frequent, commonly hazardous eruptions. Magma mixing is a process of relevance for both topics because the hybridization of mafic and felsic materials may act as an eruption trigger (e.g., Kent et al., 2010). Mineral zonation patterns that record mixing dynamics can be used to measure pre-eruptive time scales (e.g., Kahl et al., 2011), which are useful parameters for hazard mitigation efforts during modern-day eruption scenarios. Mixing is commonly described for arc volcanic rocks, including some examples of high-Mg andesite and dacite (HMAD). These are defined as having whole-rock Mg# values [$Mg\# = 100 \times Mg / (Mg + Fe)$] of ≥ 45 , higher than otherwise expected over the SiO_2 range of 54–65 wt% (Kelemen et al., 2003). While some examples of HMAD volcanism are attributed to a primary mantle origin (e.g., Bry-

ant et al., 2011), petrographic studies highlight the role of mafic-felsic magma mixing accompanied by olivine accumulation in disproportionately raising the bulk-rock Mg abundance in other cases (e.g., Streck et al., 2007). Examples of the latter type are valuable for understanding the types and time lines of crustal-level magma hybridization processes. Here we present mineralogical characteristics and orthopyroxene Fe-Mg interdiffusion time scales for a suite of HMAD lavas from Ruapehu volcano, New Zealand, a large andesite-dacite stratovolcano of the Taupo Volcanic Zone with a 200 k.y. history of effusive eruptions (Fig. 1; Conway et al., 2016).

SAMPLES AND ANALYTICAL METHODS

Samples were collected from HMAD lavas that were erupted from 48 to 37 ka onto the southern and western flanks of Ruapehu volcano (Conway et al., 2016; Fig. 1). They have whole-

rock Mg# values of 60–69 (andesites) and 53–57 (dacites), plus elevated Ni (~30–150 ppm) and Cr (~100–470 ppm) at equivalent SiO_2 contents when compared with all other lavas from Ruapehu (Conway et al., 2018; Fig. S1 in the Supplemental Material¹). Samples used for this study represent ranges in eruption age, composition, geographic distribution, and cooling rate (Table S2 in the Supplemental Material). The lavas are non- to moderately vesicular with 15%–35% macrocrystals ($>100 \mu m$). Backscattered electron (BSE) images and major-element data for minerals were collected by electron probe microanalysis. Crystal axis orientations for orthopyroxenes used for diffusion modeling were determined by electron backscatter diffraction (EBSD). See the Supplemental Material for details of analytical methods and supplementary data (Table S3).

MINERAL CHARACTERISTICS AND ORIGINS

Pyroxene

Sharply reverse-zoned orthopyroxene and clinopyroxene are ubiquitous in Ruapehu HMAD lavas (type 1 crystals; Figs. 2A and 2B). Type 1 orthopyroxene and clinopyroxene cores vary over Mg# 67–80, but individual cores are generally unzoned, slightly resorbed, and overgrown by 8–15- μm -thick rims of Mg# 82–89, with outermost higher-FeO reaction rinds. Type 1 pyroxenes occur as single euhedral or broken grains and as crystal clusters that can include ortho- and clinopyroxene (Fig. 2A). Type 2 pyroxenes are unzoned, with Mg# values

¹Supplemental Material. Details of analytical methods, and supplemental data and figures. Please visit <https://doi.org/10.1130/G47614.1> to access the supplemental material, and contact editing@geosociety.org with any questions.

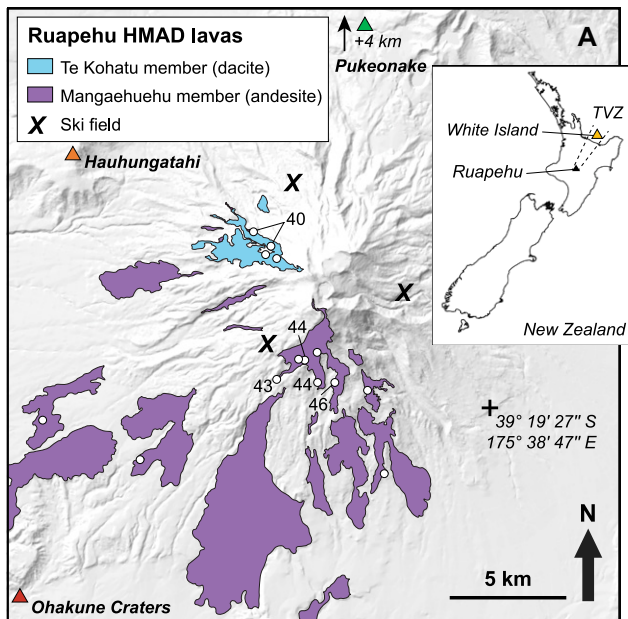
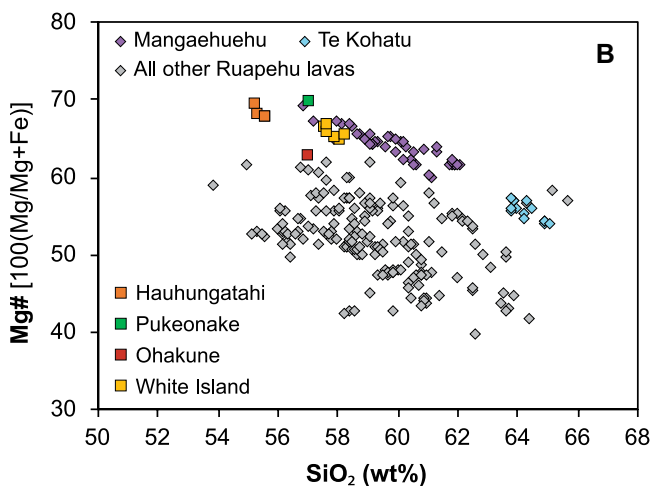


Figure 1. (A) Location of high-Mg andesite and dacite (HMAD) eruptive centers in the Taupo Volcanic Zone (TVZ), New Zealand, and distribution of HMAD lavas at Ruapehu volcano (after Conway et al., 2016). Samples used in this study are marked (circles), with ages (rounded, in ka) shown for dated samples. (B) Mg# versus SiO₂ plot of Ruapehu HMAD lavas (purple and blue diamonds) compared with other eruptives from Ruapehu (gray diamonds) and TVZ (squares). See Figure S1 (see footnote 1) for data sources.



equivalent to those of type 1 crystal cores, and commonly occur as clusters (Fig. 2C). Type 3 orthopyroxene crystals have high Mg# cores (like type 1 crystal rims) and display normal zoning toward their rims (Fig. 2D).

Several features imply that type 1 and 2 pyroxene cores were derived from a felsic source. First, average orthopyroxene (opx) core values of Mg# 75 are in equilibrium with relatively evolved melt compositions (Mg# 45), applying a Fe = Mg exchange coefficient, K_D $[(Fe/Mg)_{opx}/(Fe/Mg)_{liquid}]$, of 0.3 (Price et al., 2012), and not with host whole-rock values of Mg# 53–69. Second, type 1 orthopyroxene and clinopyroxene cores are homogeneous, consistent with subsolidus equilibration (Putirka, 2008). Third, orthopyroxene commonly occurs in multi-grain clusters, with rhyodacitic to rhyolitic melt inclusions and interstitial glass (Conway et al., 2018). This felsic source is inferred to have been largely crystalline (hereafter termed mush). Rim characteristics of type 1 pyroxenes indicate that the felsic mush was dis-

turbed, and that outer zones (and type 3 grains) grew from more primitive melts. Broken grains that lack a complete higher-Mg# rim (Fig. 2B) were likely derived from crystal clusters that were disaggregated during magma hybridization events shortly prior to eruption.

Olivine and Spinel

Type 4 crystals (mostly ~600 μ m, rarely to 4 mm) and glomerocrysts are high-forsterite (high-Fo) olivines that are anhedral, resorbed, and orthopyroxene overgrown, with abundances in samples that correlate with whole-rock Mg# (Table S2). The Fo and NiO contents of their cores indicate equilibrium with peridotitic mantle (~2500 ppm NiO at 91 mol% Fo [Fo₉₁]; Fig. S4). Rims are normally zoned (Fo_{76–86}) across ~100 μ m and slightly to moderately resorbed with adhering <100- μ m-wide rinds of type 3 orthopyroxene (Fig. 2E). Euhedral spinels, as large as 100 μ m across, are included within most type 4 olivines (Fig. 2E). They are chromian (Cr# 61–75), with Mg# 32–68, 0.2–2.0 wt% TiO₂, and

10.5–19.0 wt% Al₂O₃, indicative of a depleted arc mantle source (Fig. S4). Using overgrowth rates from Coombs and Gardner (2004) and Zellmer et al. (2016), the dimensions of orthopyroxene coronae on type 4 olivines are consistent with their mixing into felsic magma over periods of weeks to months. We infer that the olivines were carried by mantle-derived basalts (~11 wt% MgO; Barker et al., 2020) that induced the reverse-zoned growth of type 1 pyroxene rims on mixing with felsic mush in the crust. The large, anhedral and sometimes glomerocrystic nature of the olivines suggests that they were not cogenetic with the mafic magma but were instead incorporated from a preexisting cumulate body.

Olivines with Fo_{74–78} cores that show resorption and diffuse normal or no zoning and have extensive >100 μ m orthopyroxene rinds are classed as type 5 crystals (Fig. 2F). The overgrowth orthopyroxene crystals are mostly type 3, but type 1 crystals are also present (Fig. 2F). Type 5 olivines are interpreted to represent type 4 olivines that experienced prolonged crustal storage resulting in extended orthopyroxene overgrowths and diffusive reequilibration of their cores. The presence of type 1 orthopyroxene as overgrowths indicates that type 5 olivines experienced a final mixing event, consistent with there having been recurring mafic magma recharge pulses into the felsic magma bodies.

Plagioclase and Hornblende

Plagioclase is ubiquitous in the samples, with typical lengths of 300–700 μ m, and maximum lengths of 5 mm. Two prominent types show sharply defined reverse (type 6) or normal (type 7) zonation of their rims (outer ~100 μ m; Figs. 2G and 2H). Hornblende (type 8 crystals) occurs only in Te Kohatu member dacite lavas (Conway et al., 2018), reflecting more hydrous source magmas compared with the andesites (Putirka, 2016). They are 200–500- μ m-long grains, commonly with adhering plagioclase or pyroxene, and are partially to fully opacitic, with symplectitic assemblages of orthopyroxene, plagioclase, and Fe-Ti oxides replacing their outer 20–100 μ m rims (Fig. 2I). These crystals yielded an average pressure of 3.5 kbar (~13 km depth in continental crust) using the Al-in-hornblende barometer of Ridolfi et al. (2010). We tested this result against the liquid-amphibole barometer of Putirka (2016), using a melt composition similar to the least-fractionated melt inclusions in Conway et al. (2018), and refined to be in equilibrium with the amphiboles (i.e., 68.5 wt% SiO₂, 1.3 wt% MgO) using the methods of Scruggs and Putirka (2018). The resulting pressure outputs (average of 3.6 kbar; ~13 km depth) are identical to those calculated using the Ridolfi et al. (2010) model. The (partial) preservation of hornblende implies rapid magma ascent from these depths (e.g., Auer et al., 2015), thus providing a valuable constraint on the depth of mixing within the crust.

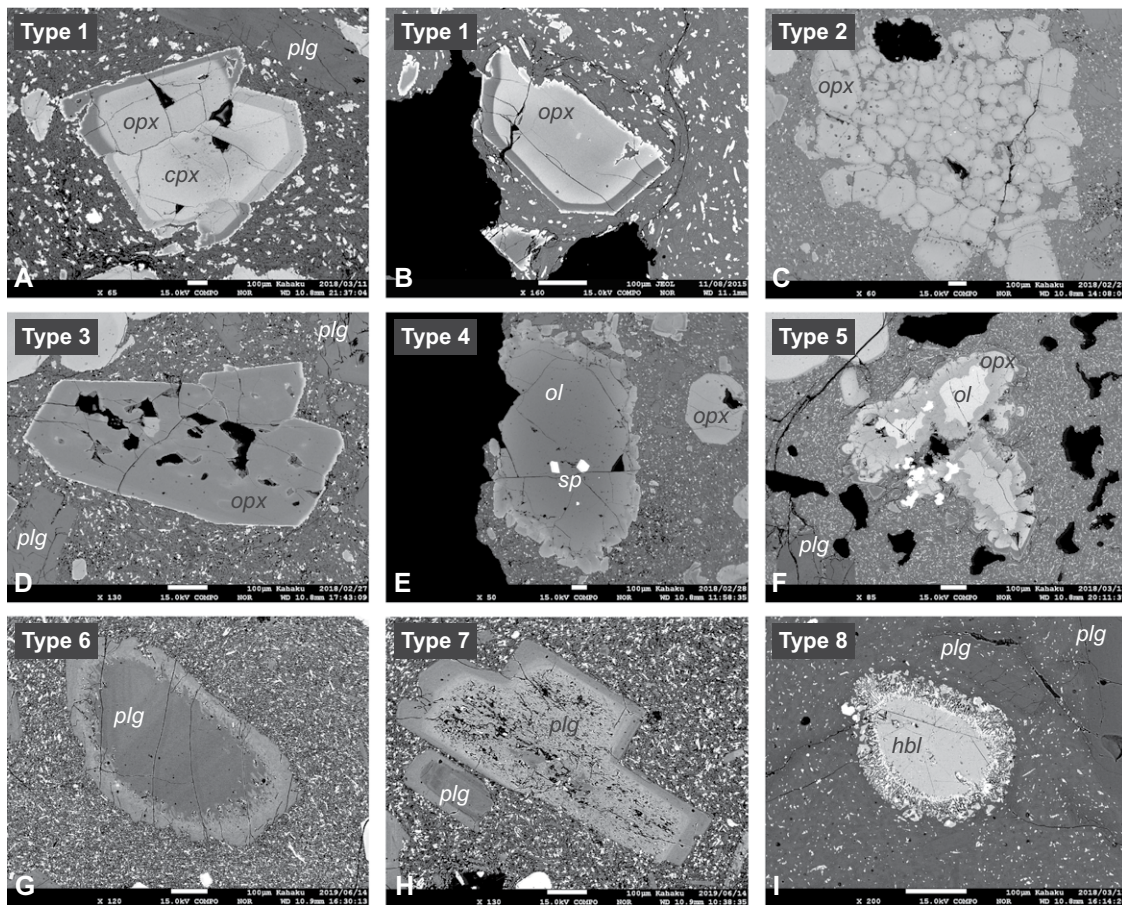


Figure 2. Backscattered electron images of crystal types within Ruapehu volcano (New Zealand) high-Mg andesite and dacite (HMAD) lavas. White scale bar in each image is 100 μm . cpx—clinopyroxene; hbl—hornblende; ol—olivine; opx—orthopyroxene; plg—plagioclase; sp—spinel.

TIME-SCALE MODELING METHODS AND RESULTS

Iron-magnesium (Fe-Mg) interdiffusion time-scale modeling was carried out on 54 core-rim boundaries in type 1 orthopyroxene crystals from five andesite samples that met the criteria for accurate modeling (Krimer and Costa, 2017) and are representative of the crystal features in all studied Ruapehu HMAD lavas. Modeling used the calibration of Ganguly and Tazzoli (1994) without an oxygen fugacity correction (after Dohmen et al., 2016) to calculate Fe-Mg interdiffusion coefficient, $D_{\text{Fe-Mg}}$, in orthopyroxene (Cooper et al., 2017). We used a two-pyroxene Fe-Mg exchange temperature of 1100 $^{\circ}\text{C}$ from the geothermometer of Putirka (2008) that was derived from 21 type 1 orthopyroxene-clinopyroxene rim pairs (Fig. S5). Finite-difference methods were used to model profiles with an assumed initial step function (full details in the Supplemental Material). EBSD analysis enabled the assessment of suitable crystal boundaries for modeling; where possible, profiles perpendicular to the *c*-axis were used (Fig. 3). Modeled time scales are from 0.4 to 27 days, with 50 of 54 crystals recording <10 days (Fig. 3D). Error reflects Monte Carlo simulations of uncertainty, which used ± 20 $^{\circ}\text{C}$ (1σ) for the temperature constraint and incorporated uncertainties relating to pixel size, the number of integrated pixel lines across each boundary, and the grayscale values used to define the Mg# values.

ORIGINS OF RUAPEHU HMAD MAGMAS

The mineralogical features (Fig. 2) and geochemical trends (Fig. S1) defined by Ruapehu HMAD samples yield a model of mixing between a mafic end member (basaltic melt with olivine xenocrysts) and a felsic end member (rhyodacitic mush bodies). Our model for Ruapehu HMAD eruptives (Fig. 4) starts with mantle-derived magmas, which incorporated olivine xenocrysts that crystallized below or at the base of the crust (>25 km depth; Salmon et al., 2011). These olivines were carried into felsic mush bodies, resulting in resorption, normal zoning, and pyroxene overgrowth over weeks to months (e.g., Coombs and Gardner, 2004). The crystal mushes likely represent the residues of magmas erupted since ca. 160 ka, which is the lower limit of ages for lavas from this part of the edifice (Gamble et al., 2003), and therefore have inferred mid-crustal (~20–9 km) loci in the central axis of the volcanic plumbing system. Seismic tomography suggests a transition to feeder dikes above this (Rowlands et al., 2005), and hornblende barometry constraints of ~13 km depth are consistent with mixing in the mid-crust (Fig. 4). We infer that mafic magma intruded and mobilized the mid-crustal storage zone: crystal mushes were disaggregated and the rims of type 1 pyroxene formed and then quenched by eruption within days to weeks. These rapidly instigated eruptions resulted in

substantial construction of the edifice (Fig. 1A). Similar petrological and geochemical features suggest a common mode of magma genesis for HMAD eruptives from White Island (Mandon, 2017), Pukeonake (Beier et al., 2017) and Hauhungatahi (Cameron et al., 2010) (Fig. 1A). Moreover, magma-mixing origins proposed for HMAD in global examples are based on similar features of xenocrystic high-Fo olivine and sharply reverse-zoned orthopyroxene and clinopyroxene (e.g., Ohba et al., 2010; Streck and Leeman, 2018), suggesting that a hybrid origin for HMAD may be widespread.

UTILITY OF DIFFUSION MODELING FOR HAZARD PREPAREDNESS

Petrochronologic studies of olivine routinely incorporate crystal-axis data due to olivine's well-defined anisotropic diffusivity tensor (e.g., Kahl et al., 2011). While diffusion anisotropy is not fully constrained for orthopyroxene (Krimer and Costa, 2017), we show here that its effects can be limited using quantitative crystal-orientation data. By analyzing thin sections, crystal-axis orientation measurements were performed rapidly by EBSD and integrated with BSE imagery and analytical data, while petrologic context was retained. Our results indicate eruptions occurred 0.4–27 days (with 50 of 54 crystals recording eruption <10 days) after the initiation of overgrowths following magma mixing events

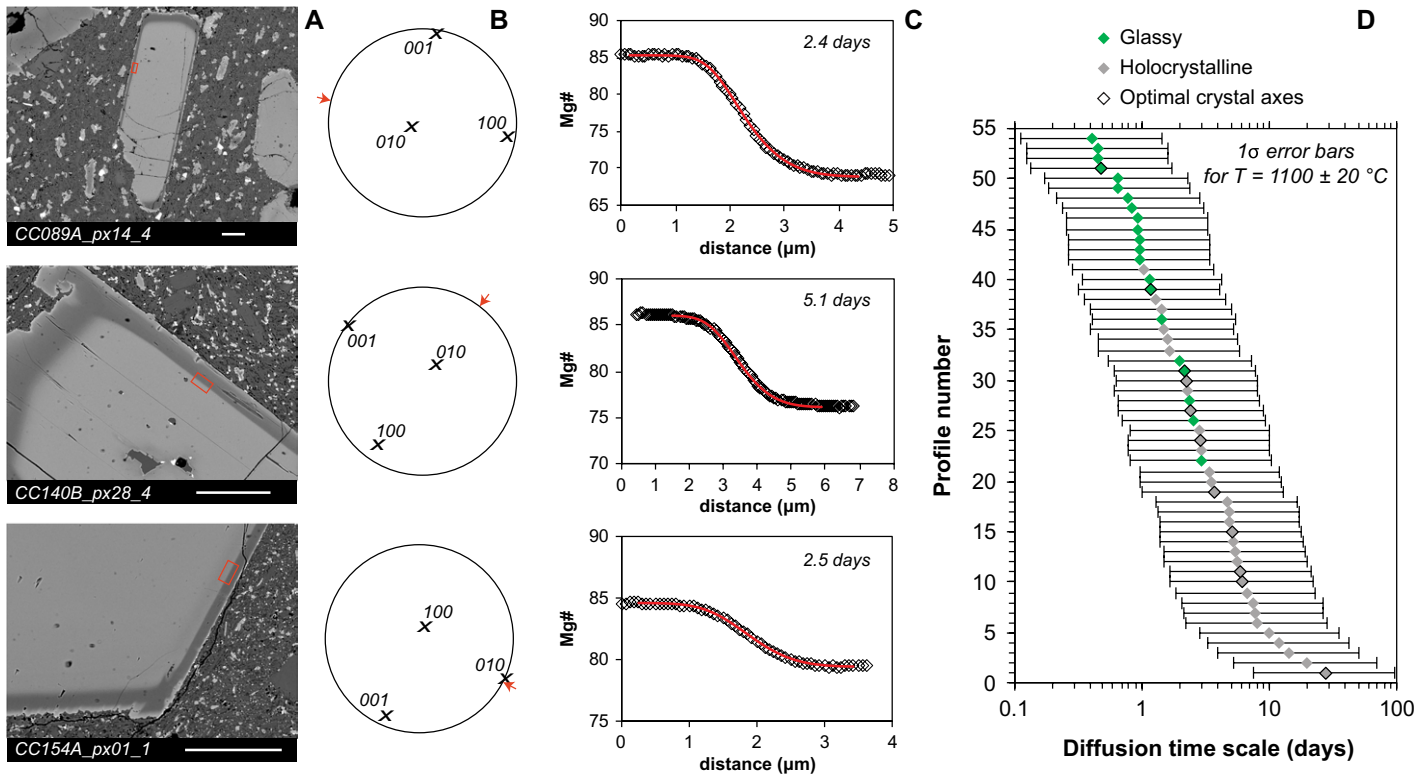


Figure 3. Exemplary crystals and results for Fe-Mg interdiffusion time-scale modeling. (A) Backscattered electron (BSE) images of analyzed crystals. Red boxes indicate area used to derive grayscale profiles. Scale bars are 100 μm . (B) Crystal-axis data from electron backscatter diffraction analyses: 100 (a-axis), 010 (b-axis) and 001 (c-axis) are displayed on equal-area, lower-hemisphere stereographic projections. Red arrow indicates trend of modeled profile. (C) Measured (black diamonds) and modeled (red line) compositional profiles. Values of Mg# [$100 \times \text{Mg} / (\text{Mg} + \text{Fe})$] were converted from grayscale intensity values derived from BSE images using electron probe microanalysis data. (D) Time-scale results determined by Fe-Mg interdiffusion modeling for type 1 orthopyroxene crystals. Results for crystals from glassy samples (green diamonds) and holocrystalline samples (gray diamonds) are distinguished, and crystals with optimal c-axis orientations for modeling are marked with black outlines. Error bars are 1σ modeling uncertainties ($T=1100 \pm 20$ $^{\circ}\text{C}$).

(Fig. 3). For optimally oriented crystals, the average time scale is 4.1 days ($n = 5$) for holocrystalline sample CC089 and 1.3 days ($n = 3$) for glassy sample CC174. This contrast holds for the full data set, with average time scales

of 5.9 days for 33 crystals from holocrystalline samples and 1.2 days for 21 crystals from glassy samples. Our data imply that post-emplacement cooling can skew short-term modeled diffusion time scales for crystals collected from the

interiors of slowly cooled lava flows. Crystals from glassy samples are more likely to record accurate magma mixing time scales unaffected by continued diffusional relaxation during lava emplacement and prolonged cooling. Our results

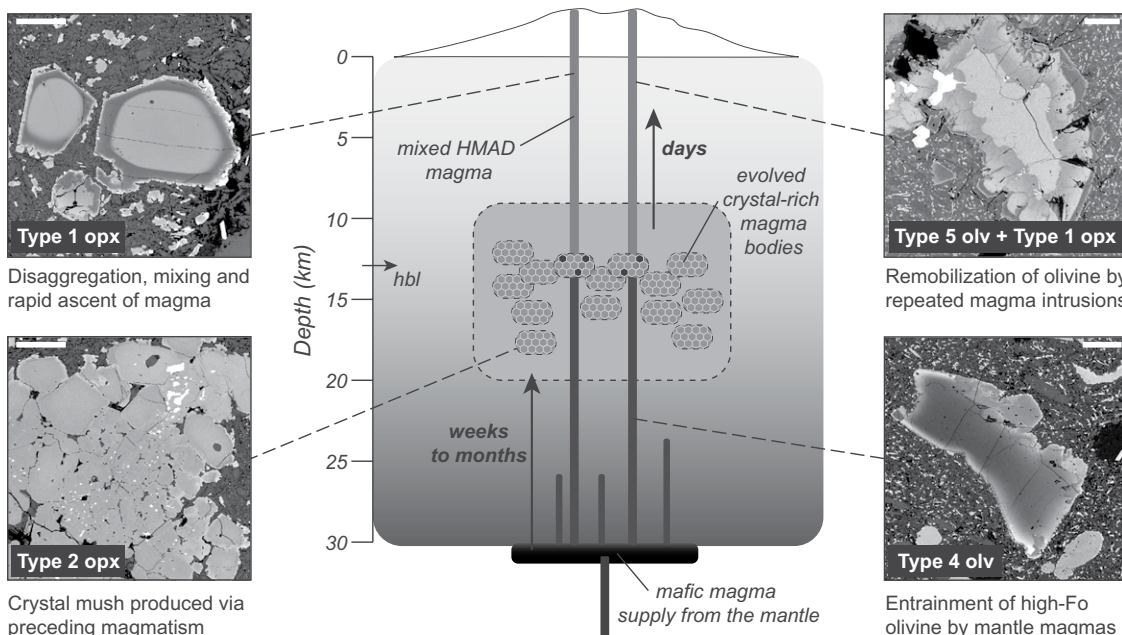


Figure 4. Schematic cross section of the magma plumbing system beneath Ruapehu volcano (New Zealand) during high-Mg andesite and dacite (HMAD) magma genesis, with exemplary backscattered electron images of key crystal types (scale bars are 100 μm). Calculated equilibration depth of hornblende (hbl) is noted. opx—orthopyroxene; olv—olivine; Fo—forsterite.

indicate that if magma ascent yields detectable geophysical signals, the eruption of lava with volumes large enough to impact local infrastructure could occur with only days of warning at Ruapehu. Although the mixing-to-eruption period occurred over days to weeks in each case, $^{40}\text{Ar}/^{39}\text{Ar}$ ages for lavas indicate that this process occurred repeatedly, with repose periods of centuries or more between successive eruptions at that time (Conway et al., 2016). Recognizing similarly recurrent patterns in future eruptive scenarios would provide greater confidence for long-term hazard forecasting.

CONCLUSIONS

We conducted a petrological and geochemical investigation of high-Mg andesite-dacite (HMAD) lava flows that were erupted at Ruapehu volcano, as a case study of rapid magma genesis and eruption at a continental arc stratovolcano. The HMAD magmas were generated by mixing between mantle-derived, high-Fo olivine-bearing mafic magmas and mid-crustal felsic mush bodies. Disruption of the mush by mafic recharge is recorded by disaggregated orthopyroxene crystals, which display sharp reverse zoning of their rims. Magma mixing-to-eruption time scales, based on Fe-Mg interdiffusion modeling constrained by crystal-orientation data, range from 0.4 to 27 days, with 50 of 54 crystals recording <10 days. Lava flows are the dominant feature of Ruapehu volcano; however, no effusive eruptions of lava onto its flank have occurred in recorded history. The rapid mobilization and eruption of mid-crustal magmas reported here provides valuable context for eruptive scenarios at active arc volcanoes and indicates that the onset of future effusive eruptions at Ruapehu may occur with very little warning.

ACKNOWLEDGMENTS

Conway was supported by postdoctoral research fellowship (P16788) and startup (19K23471) grants from the Japan Society for the Promotion of Science (JSPS). Chamberlain was supported by JSPS grant PE16724. We thank J. Gamble, S. Barker, L. Pure, K. Tani, T. Sano, and F. Hayashi for discussions and laboratory assistance, and K. Putirka and L. McGee for helpful reviews.

REFERENCES CITED

Auer, A., Martin, C.E., Palin, J.M., White, J.D.L., Nakagawa, M., and Stirling, C., 2015, The evolution of hydrous magmas in the Tongariro Volcanic Centre: The 10 ka Pahoka-Mangamate eruptions: *New Zealand Journal of Geology and Geophysics*, v. 58, p. 364–384, <https://doi.org/10.1080/00288306.2015.1089913>.

Barker, S.J., Rowe, M.C., Wilson, C.J.N., Gamble, J.A., Rooyackers, S.J., Wysoczanski, R.J., Illsley-Kemp, F., and Kenworthy, C.C., 2020, What lies beneath? Reconstructing the primitive magmas fueling voluminous silicic volcanism using olivine-hosted melt inclusions: *Geology*, v. 48, p. 504–508, <https://doi.org/10.1130/G47422.1>.

Beier, C., Haase, K.M., Brandl, P.A., and Krumm, S.H., 2017, Primitive andesites from the Taupo Volcanic Zone formed by magma mixing: Contributions to Mineralogy and Petrology, v. 172, p. 1–14, <https://doi.org/10.1007/s00410-017-1354-0>.

Bryant, J.A., Yagodinski, G.M., and Churikova, T.G., 2011, High-Mg# andesitic lavas of the Shisheisky Complex, Northern Kamchatka: Implications for primitive calc-alkaline magmatism: Contributions to Mineralogy and Petrology, v. 161, p. 791–810, <https://doi.org/10.1007/s00410-010-0565-4>.

Cameron, E., Gamble, J., Price, R., Smith, I., McIntosh, W., and Gardner, M., 2010, The petrology, geochronology and geochemistry of Hauhungatahi volcano, S.W. Taupo Volcanic Zone: *Journal of Volcanology and Geothermal Research*, v. 190, p. 179–191, <https://doi.org/10.1016/j.jvolgeores.2009.07.002>.

Conway, C.E., Leonard, G.S., Townsend, D.B., Calvert, A.T., Wilson, C.J.N., Gamble, J.A., and Eaves, S.R., 2016, A high-resolution $^{40}\text{Ar}/^{39}\text{Ar}$ lava chronology and edifice construction history for Ruapehu volcano, New Zealand: *Journal of Volcanology and Geothermal Research*, v. 327, p. 152–179, <https://doi.org/10.1016/j.jvolgeores.2016.07.006>.

Conway, C.E., Gamble, J.A., Wilson, C.J.N., Leonard, G.S., Townsend, D.B., and Calvert, A.T., 2018, New petrological, geochemical, and geochronological perspectives on andesite-dacite magma genesis at Ruapehu volcano, New Zealand: *The American Mineralogist*, v. 103, p. 565–581, <https://doi.org/10.2138/am-2018-6199>.

Coombs, M.L., and Gardner, J.E., 2004, Reaction rim growth on olivine in silicic melts: Implications for magma mixing: *The American Mineralogist*, v. 89, p. 748–759, <https://doi.org/10.2138/am-2004-5-608>.

Cooper, G.F., Morgan, D.J., and Wilson, C.J.N., 2017, Rapid assembly and rejuvenation of a large silicic magmatic system: Insights from mineral diffusive profiles in the Kidnappers and Rocky Hill deposits, New Zealand: *Earth and Planetary Science Letters*, v. 473, p. 1–13, <https://doi.org/10.1016/j.epsl.2017.05.036>.

Dohmen, R., Ter Heege, J.H., Becker, H.-W., and Chakraborty, S., 2016, Fe-Mg interdiffusion in orthopyroxene: *The American Mineralogist*, v. 101, p. 2210–2221, <https://doi.org/10.2138/am-2016-5815>.

Gamble, J.A., Price, R.C., Smith, I.E.M., McIntosh, W.C., and Dunbar, N.W., 2003, $^{40}\text{Ar}/^{39}\text{Ar}$ geochronology of magmatic activity, magma flux and hazards at Ruapehu volcano, Taupo Volcanic Zone, New Zealand: *Journal of Volcanology and Geothermal Research*, v. 120, p. 271–287, [https://doi.org/10.1016/S0377-0273\(02\)00407-9](https://doi.org/10.1016/S0377-0273(02)00407-9).

Ganguly, J., and Tazzoli, V., 1994, Fe²⁺-Mg interdiffusion in orthopyroxene: Retrieval from the data on intracrystalline exchange reaction: *The American Mineralogist*, v. 79, p. 930–937.

Kahl, M., Chakraborty, S., Costa, F., and Pompilio, M., 2011, Dynamic plumbing system beneath volcanoes revealed by kinetic modeling, and the connection to monitoring data: An example from Mt. Etna: *Earth and Planetary Science Letters*, v. 308, p. 11–22, <https://doi.org/10.1016/j.epsl.2011.05.008>.

Kelemen, P.B., Yagodinski, G.M., and Scholl, D.W., 2003, Along-strike variation in the Aleutian island arc: Genesis of high Mg# andesite and implications for continental crust, in Eiler, J., ed., *Inside the Subduction Factory: American Geophysical Union Geophysical Monograph 138*, p. 223–276.

Kent, A.J.R., Darr, C., Koleszar, A.M., Salisbury, M.J., and Cooper, K.M., 2010, Preferential eruption of andesitic magmas through recharge filtering: *Nature Geoscience*, v. 3, p. 631–636, <https://doi.org/10.1038/ngeo924>.

Krimer, D., and Costa, F., 2017, Evaluation of the effects of 3D diffusion, crystal geometry, and initial conditions on retrieved time-scales from Fe-Mg zoning in natural oriented orthopyroxene crystals: *Geochimica et Cosmochimica Acta*, v. 196, p. 271–288, <https://doi.org/10.1016/j.gca.2016.09.037>.

Mandon, C.L., 2017, Volatile transport of metals in the andesitic magmatic-hydrothermal system of White Island [Ph.D. thesis]: Wellington, New Zealand, Victoria University of Wellington, 221 p.

Ohba, T., Kimura, Y., and Fujimaki, H., 2010, High-magnesian andesite produced by two-stage magma mixing: A case study from Hachimantai, northern Honshu, Japan: *Journal of Petrology*, v. 48, p. 627–645, <https://doi.org/10.1093/petrology/egl075>.

Price, R.C., Gamble, J.A., Smith, I.E.M., Maas, R., Waight, T., Stewart, R.B., and Woodhead, J., 2012, The anatomy of an andesite volcano: A time-stratigraphic study of andesite petrogenesis and crustal evolution at Ruapehu volcano, New Zealand: *Journal of Petrology*, v. 53, p. 2139–2189, <https://doi.org/10.1093/petrology/egs050>.

Putirka, K.D., 2008, Thermometers and barometers for volcanic systems: Reviews in Mineralogy and Geochemistry, v. 69, p. 61–120, <https://doi.org/10.2138/rmg.2008.69.3>.

Putirka, K.D., 2016, Amphibole thermometers and barometers for igneous systems and some implications for eruption mechanisms of felsic magmas at arc volcanoes: *The American Mineralogist*, v. 101, p. 841–858, <https://doi.org/10.2138/am-2016-5506>.

Ridolfi, F., Renzulli, A., and Puerini, M., 2010, Stability and chemical equilibrium of amphibole in calc-alkaline magmas: An overview, new thermobarometric formulations and application to subduction-related volcanoes: Contributions to Mineralogy and Petrology, v. 160, p. 45–66, <https://doi.org/10.1007/s00410-009-0465-7>.

Rowlands, D.P., White, R.S., and Haines, A.J., 2005, Seismic tomography of the Tongariro Volcanic Centre, New Zealand: *Geophysical Journal International*, v. 163, p. 1180–1194, <https://doi.org/10.1111/j.1365-246X.2005.02716.x>.

Salmon, M.L., Stern, T.A., and Savage, M.K., 2011, A major step in the continental Moho and its geodynamic consequences: The Taranaki-Ruapehu line, New Zealand: *Geophysical Journal International*, v. 186, p. 32–44, <https://doi.org/10.1111/j.1365-246X.2011.05035.x>.

Scruggs, M.A., and Putirka, K.D., 2018, Eruption triggering by partial crystallization of mafic enclaves at Chaos Crags, Lassen Volcanic Center, California: *The American Mineralogist*, v. 103, p. 1575–1590, <https://doi.org/10.2138/am-2018-6058>.

Streck, M.J., and Leeman, W.P., 2018, Petrology of “Mt. Shasta” high-magnesian andesite (HMA): A product of multi-stage crustal assembly: *The American Mineralogist*, v. 103, p. 216–240, <https://doi.org/10.2138/am-2018-6151>.

Streck, M.J., Leeman, W.P., and Chesley, J., 2007, High-magnesian andesite from Mount Shasta: A product of magma mixing and contamination, not a primitive mantle melt: *Geology*, v. 35, p. 351–354, <https://doi.org/10.1130/G23286A.1>.

Zellmer, G.F., Sakamoto, N., Matsuda, N., Iizuka, Y., Moebis, A., and Yurimoto, H., 2016, On progress and rate of the peritectic reaction Fo + SiO₂ → En in natural andesitic arc magmas: *Geochimica et Cosmochimica Acta*, v. 185, p. 383–393, <https://doi.org/10.1016/j.gca.2016.01.005>.

Printed in USA